[20] Multiplex Analysis of Inflammatory Signaling Pathways Using a High-Content Imaging System

By MALENE BERTELSEN

Abstract

This chapter describes a robust high-content cellular screening assay to simultaneously analyze the spatiotemporal activation of three different kinase-associated signaling pathways involving NF-κB, JNK, and p38, all of which are closely implicated in proliferative and proinflammatory responses. Signal transduction is dependent on the translocation of NF-κB p65 and phosphorylated c-Jun and p38 from the cytosol to the nucleus, and fluorescent immunolabeling was used to monitor changes in their cellular distribution. Cellular screening, data acquisition, and data interpretation were conducted on the ArrayScan HCS Reader (Cellomics Inc., Pittsburgh, PA). Assay adaptation to various cellular systems is feasible when sufficient separation of the nuclear and cytosolic compartment can be achieved and if cell adhesion properties permit proper attachment to the culture plates. Substitution of NF-κB p65 and phosphorylated forms of c-Jun and p38 as targets to analyze other translocating components is possible and is limited primarily by antibody specificity and the risk of fluorescent bleed-through between emission channels. Because assay validity is particularly confounded by inadequate spectral separation of the detection dyes in multicolor labeling assays, means of eliminating or counterbalancing staining artifacts are illustrated. Also, protocol parameter settings important for imaging and image processing are described, including object identification, image exposure settings, separation of cytosolic and nuclear regions, number of cells sufficient for analysis, and the use of gating thresholds critical for cell sorting and subpopulation analysis. This assay is a useful tool to investigate the interplay between signaling pathways and the mode of action, potency, and selectivity of compound inhibition of specific target molecules in a cellular context.

Introduction

The automation of high-content biology, defined as investigations of the biological activity of biomolecules and their temporal and spatial organization in intact cells, has resulted in some of the most information-rich screening platforms available. One example is the fluorescence-based

METHODS IN ENZYMOLOGY, VOL. 414

0076-6879/06 $35.00
DOI: 10.1016/S0076-6879(06)14020-3

ArrayScan HCS reader (Cellomics Inc., Pittsburgh, PA), which is an automated high-quality image acquisition and interactive data analysis system with the capacity to extract complex sets of data from single cells or cell populations (Giuliano *et al.*, 2003). It represents a valuable and efficient tool to analyze changes in cell cycle, gene expression, cell motility, receptor internalization, and trafficking of intracellular components between various cellular compartments, while also providing information about morphological changes, off-target effects, and cellular toxicity (Gasparri *et al.*, 2004; Ghosh *et al.*, 2004; Giuliano, 2003). Because the ArrayScan HCS reader permits concurrent detection of four different fluorophores, several subcellular events can be monitored simultaneously. This chapter describes a multiplex assay to quantify the interleukin (IL)-1α-mediated spatiotemporal activation of NF-κB p65 and the stress-response mitogen-activated protein kinases p38 and c-Jun N-terminal kinase (JNK). All three signaling components play central roles in the promotion of cellular proliferation and differentiation, as well as in the induction and exacerbation of inflammatory responses (Craig *et al.*, 2000; Wada and Penninger, 2004). Not surprisingly, NF-κB p65, p38, and JNK associated signaling cascades have received considerable interest as sources of potential targets in the search for antitumor and anti-inflammatory drugs. Extensive cross talk among p38, JNK, and NF-κB signaling pathways does, however, complicate the design of selective inhibitors. For example, p38 has been reported to exert both stimulating and inhibitory effects on NF-κB-dependent gene transcription via NF-κB p65 phosphorylation, and through negative regulation of transforming growth factor-β activated kinase 1 (TAK1) stimulated IκB degradation (Cheung *et al.*, 2003; Schmeck *et al.*, 2004). Studies have also demonstrated p38-mediated blockage of JNK signaling, and c-Jun has been implicated in the transcription of NF-κB-driven genes (Chen *et al.*, 2000; Xiao *et al.*, 2004). As a tool to further investigate signaling interplay and dissect positive and negative feedback loops, we have developed a multiplex assay on the ArrayScan HCS reader where translocation of cytosolic NF-κB p65 and phosphorylated forms of c-Jun (phospho-c-Jun) and p38 (phospho-p38) to the nucleus is utilized as a measure of signal transduction (Bertelsen and Sanfridson, 2005). The optimization and validation of this multiplex assay are described thoroughly in this chapter and may serve as a template for establishing screening platforms analyzing different combinations of translocating signaling components.

Assay Procedures

The protocol used for immunofluorescence labeling of NF-κB p65, phospho-c-Jun, and phospho-p38 prior to high-content analysis closely resembles standard immunocytochemistry protocols. Accordingly, primary

(1:100–1:500 dilution) and secondary (1:250–1:1000 dilution) antibodies were titrated in order to achieve a robust window between basal and IL-1α-induced phospho-c-Jun, phospho-p38, and NF-κB p65 distribution patterns in the human cervical epithelioid carcinoma-derived HeLa cell line. Because the capacity of the applied image processing algorithm to separate individual cells for analysis is reduced significantly in wells with near confluent cells, optimization of initial cell seeding density was required. A significant IL-1α-induced effect on target translocation was achieved using 9000 cells/well while maintaining a relatively high cell count per optical field, which is essential for limiting plate scan time. The following protocol represents the optimized method for evaluation of IL-1α-stimulated NF-κB p65, phospho-c-Jun, and phospho-p38 nuclear accumulation in HeLa cells.

Immunofluorescence Labeling

1. Culture HeLa cells (American Type Culture Collection, Manassas, VA) in minimum essential medium eagle (MEME) containing 1% sodium pyruvate, 1% nonessential amino acids, and 10% fetal calf serum at 37° in humidified air/CO_2 (95%/5%) and seed log-phase cells in black-walled optically clear-bottomed 96-well Packard ViewPlates (PerkinElmer, Boston, MA) at 9×10^3 cells/well (100 μl) 18 h prior to the experiment.

2. Incubate cells in 100 μl 10 ng/ml IL-1α [Sigma, St. Louis, MO; dissolved in sterile-filtered phosphate-buffered saline (PBS) containing 0.1% bovine serum albumin (BSA)] in serum-free MEME for 20 min. To verify staining selectivity, preincubate cells with pharmacological inhibitors [dissolved in dimethyl sulfoxide (DMSO)] or vehicle (maximum 0.5% DMSO) for 1 h prior to IL-1α addition.

3. Fix cells at room temperature in 100 μl prewarmed (37°) 4% paraformaldehyde for 10 to 15 min and wash with 3×200 μl PBS by flicking off the wash buffer and gently tapping the plate on a pad of tissues.

4. Permeabilize the cells in 100 μl PBS containing 0.2% Triton X-100 for 5 min and rinse once with 200 μl PBS.

5. Block nonspecific binding sites by incubation in 100 μl PBS containing 2% BSA for 1 h prior to a 2-h incubation at room temperature with a 50-μl primary antibody mixture containing 0.45 μg/ml rabbit polyclonal antibody against p38 phosphorylated at Thr180/Tyr182 (Cell Signaling Technology, Beverly, MA), 0.5 μg/ml mouse monoclonal antibody against c-Jun phosphorylated at Ser63, and 1 μg/ml goat polyclonal anti-NF-κB p65 (Santa Cruz Biotechnology, Santa Cruz, CA) in PBS supplemented with 0.01% Tween 20 and 0.2% BSA. To verify staining specificity, immunoneutralize primary

antibodies in PBS with excess blocking peptide (8- to 10-fold over the antibody) for 3 h at 4° before immunolabeling.

6. Wash cells in 200 μl PBS containing 0.05% Tween 20 for 5 min on a shaker device and rinse twice in 200 μl PBS before a 1-h incubation at room temperature with 50 μl of secondary antibodies [Alexa Fluor 488 donkey antimouse (1/250), Alexa Fluor 555 donkey antirabbit (1/200) Alexa Fluor 680 donkey antigoat (1/100) (Molecular Probes, Leiden, The Netherlands)] in PBS supplemented with 0.01% Tween 20, 0.2% BSA, and 0.625 μg/ml Hoechst 33342 (Molecular Probes, Leiden, The Netherlands) to fluorescently label cell nuclei. Centrifuge (2000*g*, 5 min, 4°) Hoechst 33342 and Alexa-conjugated antibody stock solutions prior to use to pellet aggregates.

7. Wash the cells in 200 μl PBS containing 0.05% Tween 20 for 5 min on a shaker device and rinse twice in 200 μl PBS. Leave the last wash on the cells and seal the plate with sealing tape. Plates can be stored at 4° in the dark for several weeks or scanned immediately for high-content analysis.

High-Content Analysis

High-content analysis can be performed using a range of different bioapplications available on the ArrayScan HCS reader. They differ significantly in the extent of user-defined input parameters and the number of assay output parameters describing cell- and well-related biological features. While some require minimal user interaction and are characterized by modest flexibility, others are tailored for a multiplex approach, analyzing target expression and distribution between several cellular compartments. The latter type of analysis demands a considerably higher level of user experience in data interpretation and assay optimization. In the current protocol, high-content analysis is performed using the Molecular Translocation algorithm. This bioapplication is ideal for both multiplexing and screening by allowing a high degree of assay optimization flexibility while limiting output parameters to averages of changes in cellular target distribution. The principle behind quantification of target nuclear translocation is outlined in Fig. 1. In order to determine nuclear protein distribution in the three target channels, a nuclear region mask is created based on Hoechst DNA staining (channel 1). By expanding the nuclear region mask, while remaining within cell boundaries, a concentric ring is generated and used as an approximation of the cytosolic compartment. To ascertain that the cytosolic region mask does not exceed the cell perimeter and is separated appropriately from the nuclear region, it is recommended to perform initial experiments using 20 or 40× magnification. Moreover, this helps

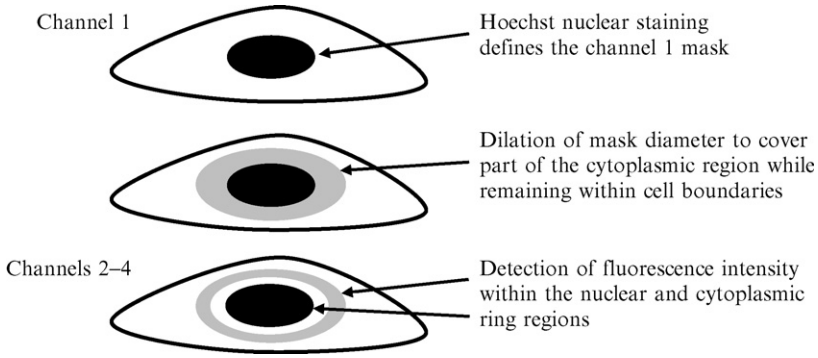

FIG. 1. Schematic of the Molecular Translocation algorithm. Based on Hoechst nuclear staining in channel 1, a nuclear mask is created, which is dilated to create a concentric ring covering part of the cytosolic compartment. The distribution of fluorescently labeled targets between nuclear and cytosolic regions is detected in channel 2–4 to measure changes in target translocation.

verify that high-content analysis output features accurately describe target distribution, target expression, and cell morphology. For screening purposes the assay may subsequently be adopted to a 5 or 10× objective lens to limit plate scan times. In the current study, using a 10× objective lens, one pixel separates the cytosolic ring from the nuclear boundary while one pixel defines the cytosolic ring width. Because cytosolic measurements are based on only a fraction of the entire cytosolic compartment, it is essential that the target is distributed homogeneously throughout the cytosol. Cytosolic and nuclear staining intensities in the target channels (channel 2–4) are normalized to total nuclear region and cytosolic ring area, allowing for the quantification of protein translocation between the nucleus and the cytosol in all three reporter channels. The difference between mean nuclear and cytosolic target staining intensities is denoted MeanNucCytDiffCh$_n$. Using the Cellomics vHCS View software, all data can, upon scan completion, be exported to an Excel spreadsheet and expressed as means ± SEM or transferred to Spotfire for further data visualization.

Image Acquisition and Object Identification

Images are captured, using a 12-bit high-resolution CCD camera, and automatically transferred to a Microsoft SQL database from where they can be retrieved easily for analysis. In the current study, images are acquired from multiple optical fields within each well in four independent channels using an Omega XF93 filter set with excitation/emission

wavelengths of 485 ± 10/515 ± 15 nm (channel 2, phospho-c-Jun), 555 ± 15/600 ± 15 nm (channel 3, phospho-p38), and 650 ± 25/725 ± 30 nm (channel 4, NF-κB p65). To ensure even field illumination, an illumination correction factor is applied, generated from measuring the illumination pattern for the filter dichroic using the illumination correction wizard. In the current protocol, Hoechst nuclear staining in channel 1 serves to identify cells as well as to optimize the focus plane. Because image overexposure is likely to prevent accurate focusing, the optimal scan exposure time in channel 1 is calculated from autoexposing three to four representative wells using a 24% upper limit for image staining saturation [Auto Exposure Options, Peak Target (percentile method)]. If Hoechst and other dye-labeled antibody aggregates have not been completely removed from the staining solution, bright specks will appear on the acquired images. Consequently, calculations are performed most accurately by excluding the upper 0.5% of the gray level image histogram (Auto Exposure settings, Skip Fraction) in both the object channel (channel 1) and the target channels (channel 2–4).

In cells characterized by a low cell to nucleus diameter ratio where the cytosolic ring domain is likely to exceed the cell perimeter, it is particularly relevant to apply fluorescence intensity thresholds to exclude background pixels from the analysis. Elongated cells represent a typical example where the cytosolic compartment in discrete areas may be too narrow to entirely omit background pixels from cytosolic ring measurements unless fluorescence intensity thresholds are specified. Object pixel identification is either performed by manually specifying an intensity threshold value (Fixed Threshold Method) or by employing an autothreshold technique based on iterative analysis of the gray level image histogram (IsoData Method). Importantly, however, if image staining is dim and object pixel intensities are approaching background intensity values, less stringent threshold measures may be required. In the current study the computed threshold values were lowered by 20% (phospho-p38; IsoData Threshold Value = −0.20) and 40% (NF-κB p65 and phospho-c-Jun; IsoData Threshold Value = −0.40) to include all pixels within the cytosolic compartment in untreated and IL-1α-stimulated cells in the analysis. To prevent erosion of the nuclear region mask and risk of inadequate separation of the nuclear and cytosolic domains, calculated Hoechst staining threshold values were reduced by 40% (IsoData Threshold Value = −0.40).

Optimization of Fluorophore Labels to Minimize Channel Bleed Through

Bleed through between reporter channels caused by insufficient spectral separation may interfere with target detection, hence representing a

potentially confounding factor in multicolor labeling assays. We have evaluated the extent of bleed through associated with secondary antibodies conjugated to Alexa Fluor 488 (channel 2), Alexa Fluor 555 (channel 3), and Alexa Fluor 680 (channel 4) dyes characterized by absorption and fluorescence emission spectra displayed in Fig. 2A. The bandwidth of the excitation and emission window of the Omega XF93 filter set is depicted in Fig. 2B, together with the extent of light transmission. Moreover, the capacity of the dichroic beam splitter to separate emitted fluorescence from scattered excitation light is indicated.

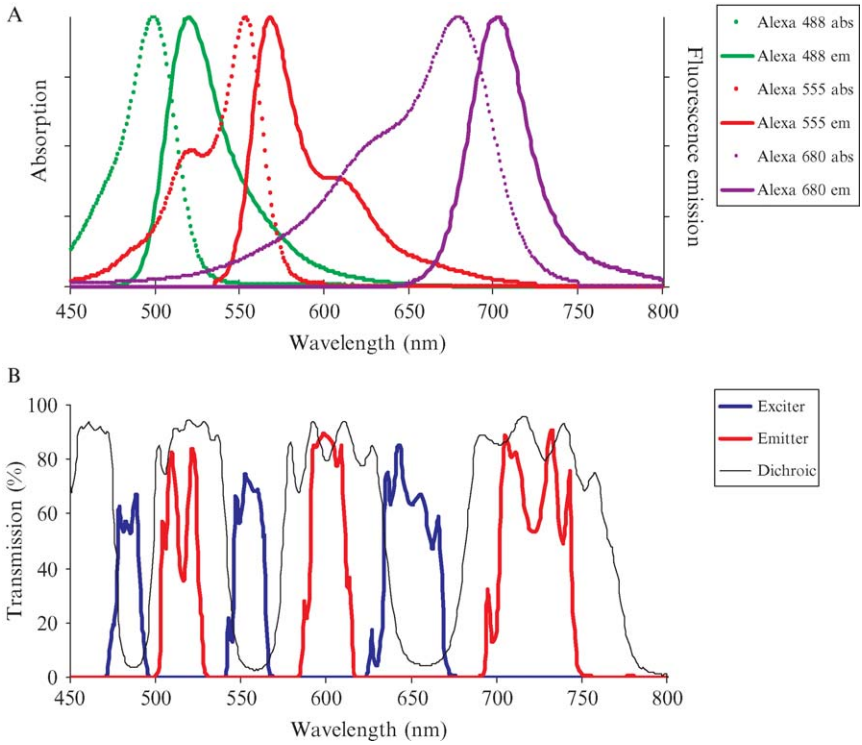

FIG. 2. Complete spectral separation of fluorophore absorption and fluorescence emission spectra with the XF93 triple-band filter set is not achievable. Absorption (stippled line, abs) and fluorescence emission (full line, em) spectra are illustrated for Alexa Fluor 488 (green), Alexa Fluor 555 (red), and Alexa Fluor 680 (purple) dyes (A). Optical transmission curves for individual XF93 filter set components are shown in blue (excitation filter), red (emission filter), and black (dichroic beam splitter) (B).

When comparing Alexa fluorophore absorbance/emission spectra with XF93 excitation/emission ranges it became clear that higher wavelength fluorophores could potentially interfere with measurements in lower wavelength reporter channels. For example, Alexa 555 and Alexa 680 are partially excited in the 485 ± 10- and 555 ± 15-nm excitation windows, respectively (Fig. 2). Although only a fraction of the resulting fluorescence emission is collected in the corresponding 515 ± 15- and 600 ± 15-nm emission windows, we found that channel bleed through had to be taken into account. The extent of bleed through was estimated using fixed target channel exposure times (phospho-c-Jun: 1.1 s; phospho-p38: 1.3 s; NF-κB p65: 5.0 s). These settings were obtained in the software interactive window by autoexposing IL-1α-stimulated cells using a maximum 25 to 30% saturation of target staining intensity [Auto Exposure Options, Peak Target (percentile method)]. If using Alexa Fluor 555 as the detection dye for phospho-c-Jun for analysis in channel 3 (Fig. 3B), significant bleed through was observed in channel 2 (Fig. 3A). Considering that bleed through from phospho-c-Jun staining was of the same magnitude as phospho-p38 MeanNucCytDiff values in channel 2 (Fig. 3A), this would clearly perturb measurements of cellular phospho-p38 distribution in a multiplexed assay. However, because the Alexa Fluor 555-derived fluorescence signal was weaker for phospho-p38 compared to phospho-c-Jun, bleed-through interference could be resolved. If interchanging the Alexa Fluor dyes associated with the secondary antibodies in order to detect phospho-c-Jun in channel 2 (Fig. 3C) and phospho-p38 in channel 3 (Fig. 3D), channel bleed through was negligible.

Because NF-κB p65 is very abundant, the less bright Alexa 680-conjugated fluorophore was chosen to track NF-κB p65 spatial responses. However, bleed through was evident in channel 3, which could only partly be compensated for by reducing the concentration of the Alexa Fluor 680 dye. For example, phospho-p38 MeanNucCytDiff values in IL-1α-stimulated cells were increased by 25 to 30% as a result of Alexa Fluor 680 dye bleed through (data not shown). This issue was overcome because a linear relationship exists between Alexa Fluor 680 staining in channels 3 and 4, provided the image is not overexposed. Thus, if using fixed exposure times in both channels, a bleed-through correction curve can be constructed by measuring the level of staining filtering through to channel 3 in cells labeled exclusively with increasing concentrations of anti-NF-κB p65 antibodies and stained with Alexa Fluor 680-conjugated antibodies (Fig. 3E, $R = 0.989$). When subsequently measuring NF-κB p65-dependent staining in the multiplex assay using fixed exposure times in both channels, it is possible to manually estimate the extent of bleed through collected in channel 3 and hence calculate true phospho-p38 staining.

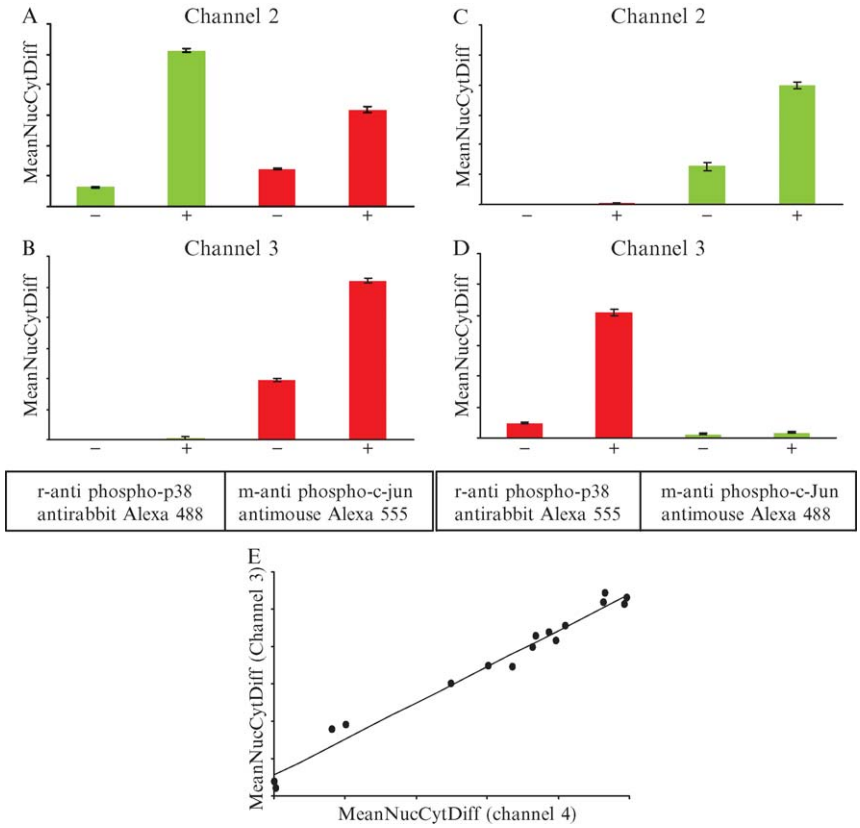

FIG. 3. Careful reporter channel selection is critical to avoid screening artifacts. HeLa cells were incubated with vehicle (−) or 10 ng/ml IL-1α (+) for 20 min prior to fixation, permeabilization, and incubation with either rabbit (r) antiphospho-p38 or mouse (m) antiphospho-c-Jun antibodies. Cells were immunolabeled with antirabbit Alexa Fluor 488 antibodies (green bars, A, B), antimouse Alexa Fluor 555 antibodies (red bars, A, B), antirabbit Alexa Fluor 555 antibodies (red bars, C, D), or antimouse Alexa Fluor 488 antibodies (green bars, C, D) prior to imaging on the ArrayScan HCS reader. The Molecular Translocation algorithm was used to calculate MeanNucCytDiff values from images collected in channel 2 (excitation: 485 $\pm$ 10 nm) (A, C) and channel 3 (excitation: 555 $\pm$ 15 nm) (B, D). In cells incubated exclusively with increasing concentrations of antigoat NF-κB p65 antibodies and labeled with Alexa Fluor 680-conjugated antigoat antibodies, the relationship between target staining in channel 4 and bleed-through staining in channel 3 is depicted (E) (adapted from Bertelsen and Sanfridson, 2005).

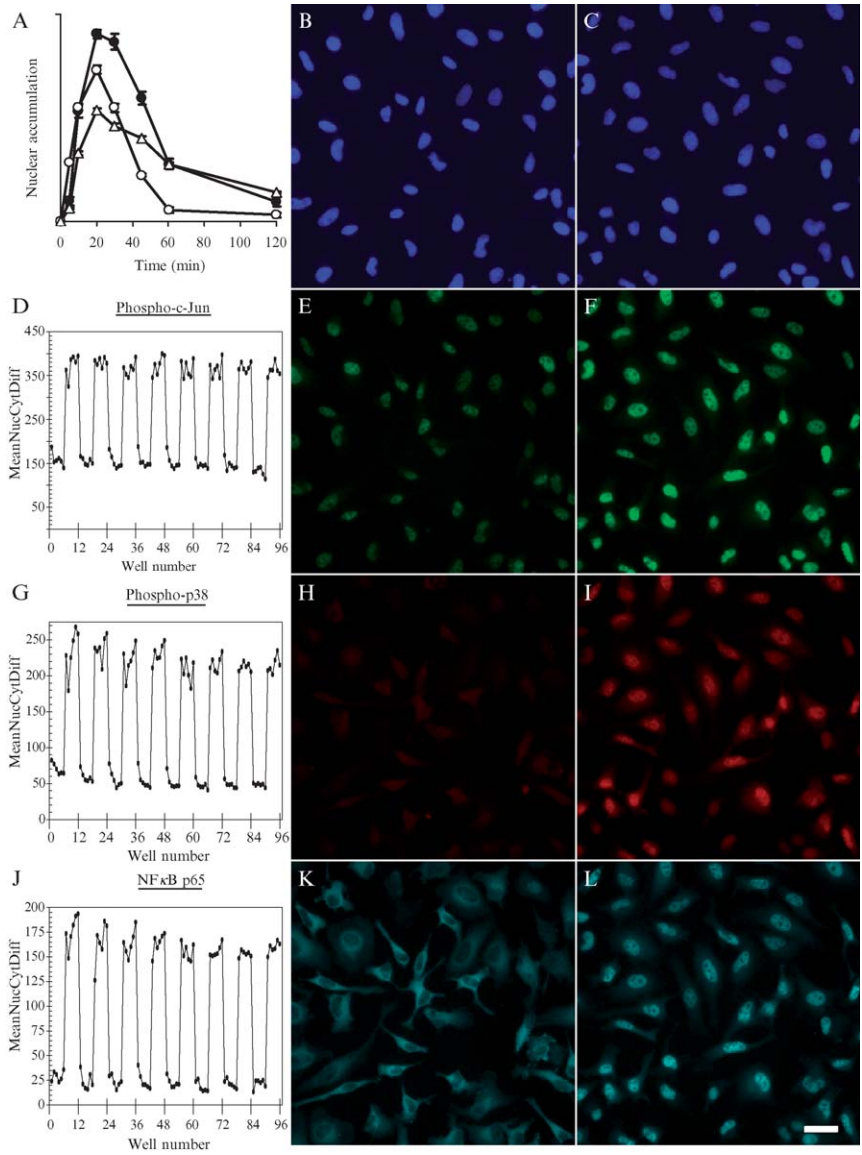

FIG. 4. IL-1α stimulates nuclear accumulation of phospho-c-Jun, phospho-p38, and NF-κB p65. HeLa cells were incubated with vehicle (B, E, H, K) or 10 ng/ml IL-1α (C, F, I, L) for 20 min prior to fixation, permeabilization, Hoechst nuclear staining (B, C), and immunolabeling with antibodies targeting phospho-c-Jun (E, F), phospho-p38 (H, I), and NF-κB p65 (K, L). Cells were imaged on the ArrayScan HCS reader using a 20× objective lens with each column reflecting images collected from the respective fluorescent channels using the same optical

Imaging Intracellular Target Distribution

The temporal sequence of IL-1α-mediated NF-κB p65, phospho-c-Jun, and phospho-p38 redistribution demonstrates a peak in target nuclear accumulation following a 20-min IL-1α exposure (Fig. 4A). This time point was subsequently used to ensure the most robust screening assay for analyzing changes in target distribution. Representative images are shown of Hoechst-stained nuclei in vehicle (Fig. 4B) and IL-1α (Fig. 4C) exposed cells captured using a 20$\times$ objective lens. Basal phospho-c-Jun levels were significant and mainly confined to the nuclear compartment (Fig. 4E), which may be associated with a putative role of phospho-c-Jun in cell cycle progression in exponentially growing cells (Bakiri *et al.*, 2000). IL-1α treatment further induced nuclear phospho-c-Jun accumulation (Fig. 4F), increasing MeanNucCytDiff measurements 2.5-fold (Fig. 4D), which was calculated from a 96-well plate where columns 1–6 were incubated with vehicle and columns 7 to 12 were stimulated with 10 ng/ml IL-1α. Untreated cells displayed a uniform phospho-p38 staining pattern just above background signal (Fig. 4H). The capacity of IL-1α to promote phospho-p38 nuclear translocation (Fig. 4I) was illustrated by a 4.7-fold increase in MeanNucCytDiff values (Fig. 4G). Finally, a typical NF-κB p65 distribution pattern was observed (Handa *et al.*, 2004), with the vast majority of the transcription factor present throughout the cytosolic compartment before stimulation (Fig. 4K), followed by a 16.5-fold increase in NFκB p65 nuclear translocation upon IL-1α treatment (Fig. 4J and 4L).

The abundance and cellular distribution pattern of all three targets were also analyzed in the lung epithelial cell line NCI-H292. Although NCI-H292 cells have a tendency to grow in multilayered clusters, which prohibits proper focusing, this issue was of limited extent if using an initial cell seeding density of 10,000 cells/well. A comparable response to IL-1α for all three proteins was observed in HeLa and NCI-H292 cells (data not shown), demonstrating the utility of this assay in other cellular systems.

Evaluation of Assay Reliability

To determine the suitability of the assay as a screening tool, the Z' factor was calculated for all three targets from means of measurements and

field. The temporal sequence of 10 ng/ml IL-1α-stimulated phospho-c-Jun (●), phospho-p38 (○), and NF-κB p65 (△) nuclear accumulation is depicted (A). MeanNucCytDiff measurements were calculated using the Molecular Translocation algorithm from a 96-well plate where columns 1–6 were incubated with vehicle and columns 7–12 were incubated with IL-1α for 20 min. Cellular distribution of phospho-c-Jun (D), phospho-p38 (G), and NF-κB p65 (J) is depicted. Scale bar: 40 μm (adapted from Bertelsen and Sanfridson, 2005).

standard deviation from measurements on vehicle and IL-1α-treated cells (Fig. 4D, 4G, and 4J) according to the method of Zhang *et al.* (1999). In the current study, a minimum of 200 cells/well were imaged using a 10× objective lens, resulting in a scanning time of approximately 45 min to complete a full 96-well plate scan. This protocol produced Z' values of 0.69 (phospho-c-Jun), 0.59 (phospho-p38), and 0.65 (NF-κB p65) if omitting outer wells often associated with lower cell densities and altered target translocation kinetics (inclusion of outer wells reduced the Z' factors by 0.1–0.2). Increasing the number of cells included for analysis to 400 cells/well merely prolonged plate scan times without enhancing assay robustness significantly. A recent study addressing microplate edge effects in cell-based assays documented that thermal gradients during cell adhesion are most pronounced in the outer wells of the plate, resulting in uneven cell distribution, possibly affecting cell responsiveness (Lundholt *et al.*, 2003). A brief preincubation period at ambient conditions prior to placement in the CO_2 incubator, as suggested by the authors, may therefore lower whole plate data variation and further improve assay reliability as a result of a more even cell distribution profile.

In order to verify the specificity of target recognition, nuclear target translocation was analyzed following pharmacological inhibition of JNK, p38, and IκB kinase (IKK2/IKKβ) activity. IKK2 constitutes part of the IKK complex responsible for phosphorylating the inhibitory subunit IκB, thereby targeting it for degradation, which results in the unmasking of the NF-κB nuclear localization signal. Cellular redistribution of phospho-c-Jun, phospho-p38, and NF-κB p65 was inhibited in a dose-dependent manner by SP600125 ($IC_{50} = 6.8\ \mu M$), SB203580 ($IC_{50} = 1.4\ \mu M$), and a specific IKK2 inhibitor ($IC_{50} = 0.4\ \mu M$), respectively (Bertelsen and Sanfridson, 2005). Further evidence supporting staining specificity was provided by antibody immunoneutralization where blocking peptides against antibodies targeting phospho-p38 and NF-κB p65 eliminated IL-1α-mediated target nuclear accumulation (data not shown). A commercially available antiphospho-c-Jun antibody-blocking peptide could not be obtained. However, a similar IL-1α redistribution response was observed using an antibody raised against a different synthetic phospho-peptide in rabbit, thus supporting monoclonal antiphospho-c-Jun antibody specificity.

Output Parameters Related to Cell Health

Several output features inherent to the Molecular Translocation algorithm are relevant for monitoring general cell health. These include average cell count/well and measures of nuclear morphology, such as nuclear size (NucArea), shape (NucShapeP2A and NucShapeLWR), and fluorescence

intensity (NucTotalIntenCh1 and NucAvgIntenCh1). Reductions in average nuclear fluorescence intensity, indicative of DNA degradation, together with nuclear condensation and fragmentation, are all indicators of cellular toxicity. Measurements of nuclear fragmentation are not offered by the Molecular Translocation algorithm; however, images can be reanalyzed using the Cell Health Profiling algorithm where Hoechst staining variability within each nucleus is calculated as a measure of nuclear integrity (MeanObject VarIntenCh1). In the current study, no apparent indications of inhibitor or IL-1α-related cell toxicity were observed. However, to obtain a more thorough cell health profile, additional indicators of cellular toxicity have to be evaluated. These may include changes in mitochondrial transmembrane potential, release of cytochrome c from mitochondria, caspase activation, F-actin reorganization, and increased cell permeability (Rudner *et al.*, 2001; van Engeland *et al.*, 1997). Examples of an ArrayScan-based multiplex approach to analyze several of these parameters have been described and demonstrated to aid understanding of the cellular mechanism of compound toxicity (Abraham *et al.*, 2004; Lovborg *et al.*, 2004).

The output features of the Molecular Translocation algorithm have been optimally tailored to report on average changes in cellular target distribution within the entire cell population. In contrast, nuclear morphology measurements are provided on an individual cell basis and not as a well average. To obtain a clear notion of cell health status, additional data analysis steps are therefore required, which may be a disadvantage in large compound screens. Alternatively, high-content analysis can be performed using the more flexible and information-rich Compartmental Analysis algorithm, which provides average well-level nuclear intensity and size measurements. Protocol settings relating to object identification and image acquisition are interchangeable between the Molecular Translocation and the Compartmental Analysis algorithms. In addition to reporting on differences in average pixel intensity between nuclear and cytosolic mask regions (CircRingAvgIntenDiff), this bioapplication also provides average target intensity measurements within either the cytosolic (RingAvgInten) or the nuclear (CircAvgInten) region. These parameters may be useful in order to elucidate if decreased target nuclear accumulation is, in part, a result of reduced cellular target expression.

Subpopulation Analysis

Because images and data are collected for each individual cell, it is possible to select or reject cells or cell populations based on morphological features or the presence of a particular marker. Initially, cells are elected for further analysis based on object identification (nuclei in the current protocol) and selection settings in channel 1. Cells are rejected if failing to

meet object identification isodata thresholds requirements (described in the Image acquisition and object identification section) or if not within a defined range for nuclear intensity, area, and shape. Subpopulation analysis is subsequently performed based on intensity measurements (AvgIntenCh$_n$, TotalIntenCh$_n$) in target channels 2–6. For example, by adjusting object selection intensity criteria in the FITC channel it is possible to monitor changes in target expression or distribution in cells transfected with a GFP-labeled marker while gating out nontransfected cells from the analysis. Alternatively, it may be of interest to analyze cellular readouts in a subpopulation not associated with phosphorylation or expression of a particular fluorescently labeled protein. This may be appropriate if analyzing cells transfected with small interfering RNA (siRNA). Because transfection efficiency is generally less than 100%, only cells with a strong siRNA uptake and significant target knockdown are relevant to include in the analysis. Based on immunolabeling of the siRNA target, subpopulation analysis is performed by lowering the maximum value of the object selection parameters; AvgIntenCh$_n$ and TotalIntenCh$_n$ in the interactive window. The object selection parameters are determined most conveniently by moving the cursor over an acquired image in the interactive window and monitoring pixel intensity, characterized by a 12-bit (0−4095) dynamic range, at the bottom of the screen.

Several of the bioapplications, including the Molecular Translocation algorithm, have the capacity to compare cellular responses to a control population typically derived from nonstimulated cells. Upper and lower thresholds defining specific features of the control population are either manually specified or computed from Reference Wells, which also provide the benefit of limiting run-to-run variation. Homogeneous control cell populations are characterized by normal physiological distribution histograms where approximately 95% of the cells fall within 2 (correction coefficient, CC) standard deviations of the mean. Distribution histograms describing different cellular features are visualized easily using the Cell Detail function in the Cellomics vHCS View software. In the current study, vehicle-treated cells were used as reference wells and lower and upper thresholds for MeanNucCytDiff values were defined using a correction coefficient of 2 in all target channels. In 86% of the cell population, IL-1α-stimulated phospho-p38 and NF-κB p65 nuclear accumulation was significantly higher compared to control (%HighCircRingAvgInten DiffCh$_n$), whereas only 70% of the cells displayed statistically higher phospho-c-Jun nuclear levels. If calculating the percentage of cells characterized by significantly induced phospho-c-Jun translocation, as well as significant nuclear accumulation of phospho-p38, NF-κB p65, or both (%HighCombinedAvgIntenDiffCh$_n$Ch$_n$), it was evident that phospho-c-Jun redistribution was always accompanied by both phospho-p38 and NF-κB p65 translocation.

Concluding Remarks

In summary, the multiplex assay described in this chapter is an example of an information-rich screening tool used to analyze the spatial and temporal distribution of signaling components in intact cells as a measure of biological activation. In contrast to biochemical model systems, this assay offers information about compound-associated cell toxicity and biological potency where the complex effects of signaling interplay are taken into account. Adapting the assay to other cell types has been demonstrated successfully, but requires that protein and phosphorylation levels of p38, c-Jun, and NF-κB p65 are analyzed carefully to reveal possible staining artifacts due to emission channel bleed through. The assay can be modified to track cellular redistribution of different combinations of signaling components, provided that antibody specificity is evaluated thoroughly. Establishing assays on the ArrayScan reader to analyze cellular responses in suspension cells or semiadherent cells represents a particular challenge and is beyond the scope of this chapter. However, the use of binding matrixes, such as collagen, poly-L-lysine, fibronectin, vitronectin, and laminin, is likely to help facilitate cell attachment to the culture plates. It is, however, critical to perform appropriate control experiments to ascertain the reliability of data, as cell–matrix interactions may induce cell activation and initiate detrimental cellular effects (Tang *et al.*, 1998).

In conclusion, we feel that this type of multiplex assay can be modified and expanded easily to generate useful cellular information, which would benefit a wide variety of drug discovery and signal elucidation projects.

Acknowledgments

I am grateful to Dr. Annika Sanfridson for helpful discussions and critical review of the manuscript. I also thank Dr. Britt-Marie Kihlberg for critical reading and comments.

References

Abraham, V. C., Taylor, D. L., and Haskins, J. R. (2004). High content screening applied to large-scale cell biology. *Trends Biotechnol.* **22,** 15–22.

Bakiri, L., Lallemand, D., Bossy-Wetzel, E., and Yaniv, M. (2000). Cell cycle-dependent variations in c-Jun and JunB phosphorylation: A role in the control of cyclin D1 expression. *EMBO J.* **19,** 2056–2068.

Bertelsen, M., and Sanfridson, A. (2005). Inflammatory pathway analysis using a high content screening platform. *Assay Drug Dev. Technol.* **3,** 261–271.

Chen, G., Hitomi, M., Han, J., and Stacey, D. W. (2000). The p38 pathway provides negative feedback for Ras proliferative signaling. *J. Biol. Chem.* **275,** 38973–38980.

Chefung, P. C., Campbell, D. G., Nebreda, A. R., and Cohen, P. (2003). Feedback control of the protein kinase TAK1 by SAPK2a/p38alpha. *EMBO J.* **22,** 5793–5805.

Craig, R., Larkin, A., Mingo, A. M., Thuerauf, D. J., Andrews, C., McDonough, P. M., and Glembotski, C. C. (2000). p38 MAPK and NF-κ B collaborate to induce interleukin-6 gene expression and release: Evidence for a cytoprotective autocrine signaling pathway in a cardiac myocyte model system. *J. Biol. Chem.* **275,** 23814–23824.

Gasparri, F., Mariani, M., Sola, F., and Galvani, A. (2004). Quantification of the proliferation index of human dermal fibroblast cultures with the ArrayScan high-content screening reader. *J. Biomol. Screen.* **9,** 232–243.

Ghosh, R. N., Grove, L., and Lapets, O. (2004). A quantitative cell-based high-content screening assay for the epidermal growth factor receptor-specific activation of mitogen-activated protein kinase. *Assay Drug Dev. Technol.* **2,** 473–481.

Giuliano, K. A. (2003). High-content profiling of drug-drug interactions: Cellular targets involved in the modulation of microtubule drug action by the antifungal ketoconazole. *J. Biomol. Screen.* **8,** 125–135.

Giuliano, K. A., Haskins, J. R., and Taylor, D. L. (2003). Advances in high content screening for drug discovery. *Assay Drug Dev. Technol.* **1,** 565–577.

Handa, O., Naito, Y., Takagi, T., Shimozawa, M., Kokura, S., Yoshida, N., Matsui, H., Cepinskas, G., Kvietys, P. R., and Yoshikawa, T. (2004). Tumor necrosis factorα-induced cytokine-induced neutrophil chemoattractant-1 (CINC-1) production by rat gastric epithelial cells: Role of reactive oxygen species and nuclear factor-κB. *J. Pharmacol. Exp. Ther.* **309,** 670–676.

Lovborg, H., Nygren, P., and Larsson, R. (2004). Multiparametric evaluation of apoptosis: Effects of standard cytotoxic agents and the cyanoguanidine CHS 828. *Mol. Cancer Ther.* **3,** 521–526.

Lundholt, B. K., Scudder, K. M., and Pagliaro, L. (2003). A simple technique for reducing edge effect in cell-based assays. *J. Biomol. Screen.* **8,** 566–570.

Rudner, J., Lepple-Wienhues, A., Budach, W., Berschauer, J., Friedrich, B., Wesselborg, S., Schulze-Osthoff, K., and Belka, C. (2001). Wild-type, mitochondrial and ER-restricted Bcl-2 inhibit DNA damage-induced apoptosis but do not affect death receptor-induced apoptosis. *J. Cell Sci.* **114,** 4161–4172.

Schmeck, B., Zahlten, J., Moog, K., van Laak, V., Huber, S., Hocke, A. C., Opitz, B., Hoffmann, E., Kracht, M., Zerrahn, J., Hammerschmidt, S., Rosseau, S., Suttorp, N., and Hippenstiel, S. (2004). Streptococcus pneumoniae induced p38 MAPK dependent phosphorylation of RelA at the interleukin-8 promotor. *J. Biol. Chem.* **279,** 53241–53247.

Tang, M. J., Hu, J. J., Lin, H. H., Chiu, W. T., and Jiang, S. T. (1998). Collagen gel overlay induces apoptosis of polarized cells in cultures: Disoriented cell death. *Am. J. Physiol.* **275,** C921–C931.

van Engeland, M., Kuijpers, H. J., Ramaekers, F. C., Reutelingsperger, C. P., and Schutte, B. (1997). Plasma membrane alterations and cytoskeletal changes in apoptosis. *Exp. Cell Res.* **235,** 421–430.

Wada, T., and Penninger, J. M. (2004). Mitogen-activated protein kinases in apoptosis regulation. *Oncogene* **23,** 2838–2849.

Xiao, W., Hodge, D. R., Wang, L., Yang, X., Zhang, X., and Farrar, W. L. (2004). NF-κB activates IL-6 expression through cooperation with c-Jun and IL6-AP1 site, but is independent of its IL6-NFkappaB regulatory site in autocrine human multiple myeloma cells. *Cancer Biol. Ther.* **3,** 1007–1017.

Zhang, J. H., Chung, T. D., and Oldenburg, K. R. (1999). A simple statistical parameter for use in evaluation and validation of high throughput screening assays. *J. Biomol. Screen.* **4,** 67–73.